

## Supporting Information

# Nontraditional Template Synthesis of Microjagged Bismuth Oxide: A Highly Efficient Visible Light Responsive Photocatalyst

Zhanglian Xu,<sup>\*[a]</sup> Isao Tabata,<sup>[a]</sup> Kazumasa Hirogaki,<sup>[a]</sup> Kenji Hisada,<sup>[a]</sup> Tao Wang,<sup>[b]</sup> Sheng Wang<sup>[b]</sup> and Teruo Hori<sup>[a]</sup>

[a]Fiber Amenity Engineering Course, Graduate School of Engineering, University of Fukui, 3-9-1, Bunkyo, Fukui-shi, Fukui-prefecture, 910-8507, Japan

[b]Key Laboratory of Advanced Textile Materials and Manufacturing Technology, Ministry of Education of P. R. China, Zhejiang Sci-Tech University, Hangzhou 310018, P. R. China

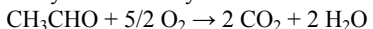
### [1] Experimental section:

#### Synthesis of free-standing Bi<sub>2</sub>O<sub>3</sub> with 3D jagged morphology and relative H<sub>2</sub>O<sub>2</sub>-treated samples:

In a typical process, Bi(NO<sub>3</sub>)<sub>3</sub>·5H<sub>2</sub>O (0.97 g, 2 mmol) and WO<sub>3</sub> (0.187 g, 1 mmol) powders were dissolved into 40 ml distilled water. After the mixture was ultrasonicated for about 30 min, the mixed solution was transferred to a Teflon-lined stainless steel autoclave with a capacity of 100 mL and put into a pre-heated oven and kept at 180 °C for 24h. After reaction, the obtained precipitates were filtered and washed with distilled water several times and dried in air at room temperature. After drying, the WO<sub>3</sub> template was removed by selective dissolution in a 5 M NaOH solution at 95 °C for 24h to yield free-standing Bi<sub>2</sub>O<sub>3</sub> photocatalysts. The as-prepared Bi<sub>2</sub>O<sub>3</sub> samples were subsequently immersed into 30 % H<sub>2</sub>O<sub>2</sub> solution and washed sufficiently to ensure no residual H<sub>2</sub>O<sub>2</sub> in samples, and the final H<sub>2</sub>O<sub>2</sub>-treated Bi<sub>2</sub>O<sub>3</sub> with different surface Bi<sub>2</sub>O<sub>4-x</sub> content can be obtained at different immersion time.

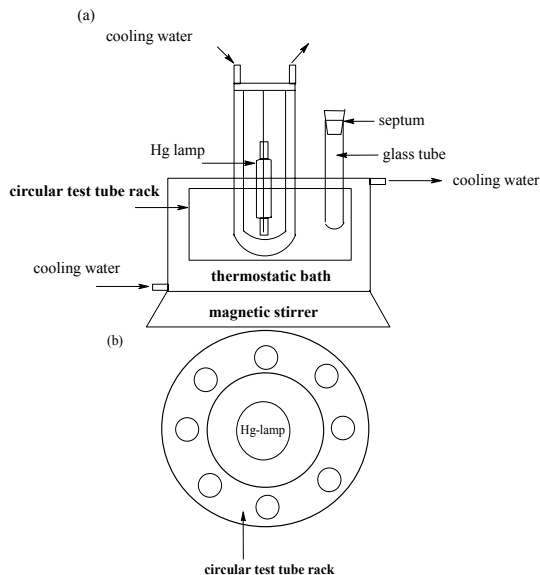
**Characterization:** A Hitachi S-4800 field emission scanning electron microscope (FESEM, Hitachi CO. Ltd. S-4800) was utilized to the morphology investigation. TEM images were collected by using a JEOL JEM 2010F microscope working at 200 kV. X-ray diffraction (XRD, Rigaku D/Max-2550pc) measurements were carried out using filtered Cu K $\alpha$  radiation. Energy dispersive X-ray analysis (EDXA, Inca Energy-200) is used to investigate the sample composition. A Shimadzu UV-1601PC spectrophotometer was used to record the UV-vis spectra of the sample. The chemical state transition of surface element was determined by X-ray Photoelectron Spectroscopy (XPS, JEOL, JPS-9010MCY)

**Photocatalytic activity measurement:** The overall photocatalytic activity was tested as the amounts of CO<sub>2</sub> gas that generated from the oxidation decomposition of aqueous acetaldehyde solution (0.25 vol%, ca.85  $\mu$ mol) containing a suspension of the photocatalyst powder (40 mg) under the irradiation of UV lamp with the cutoff filters ( $\lambda > 400$  nm and  $\lambda > 320$  nm) at 25°C. The irradiation intensity measured by radiometer between 320 to 380 nm was about 8% in the total spectrum of UV lamp. For photocatalysis experiments, the rate of agitation was set at 700 rpm. The reaction stoichiometry of acetaldehyde solution has been ascertained to be following:



The CO<sub>2</sub> concentrations were measured using a gas chromatography (Align model GC-6890N) equipped with a 2 m Porapak-Q column, a methanizer, and a flame ionization detector, using N<sub>2</sub> as the carrier gas.

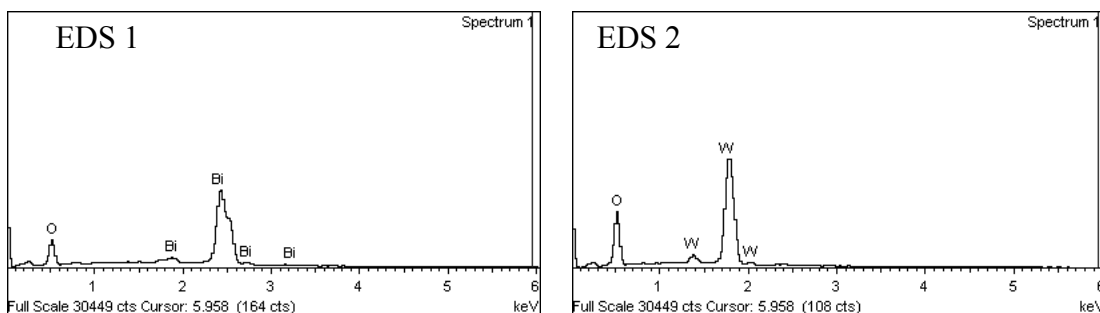
**Photocatalytic reactor:** A photocatalytic reactor was used in this study and the schematic details are depicted in Scheme S1. An ultrahigh-pressure Hg lamp (500 W) was located in the center of the reactor along the axis and protected by a water-cooled quartz jacket. At the bottom of the reactor a magnetic stirrer was used to achieve effective dispersion agitating mechanically. A circular test tube rack was inserted on the thermostatic bath to hold up the Pyrex glass tubes. Thus the UV light was collected into the glass tube and ensured the photocatalytic reaction performed uniformly and completely. The reactor was fitted with a magnetic stirrer for stirring at 700 rpm to keep the catalyst in suspension.



**Scheme S1.** The schematic illustration of the cylindrical photocatalytic reactor: (a) cross-sectional view, (b) top view.

## [2] EDXA analysis

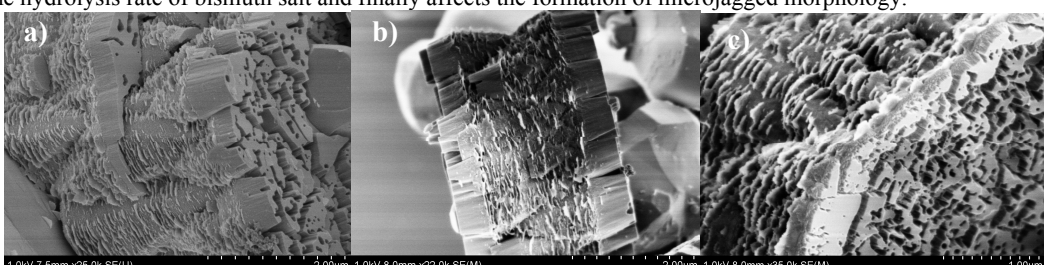
Composition of the 3D superstructure in different parts was checked using an X-ray energy spectrometer (EDS). The body of the peak part is composed of Bi and O with the ratio of Bi to O approximately equal to 2:3 (EDS1), conforming to the chemical formula of  $\text{Bi}_2\text{O}_3$ . The coronal part, however, shows the presence of W and O with the ratio of 1:3 in EDS2. That is to say, the whole component unit is made up of  $\text{WO}_3$  in the coronal and  $\text{Bi}_2\text{O}_3$  in the peak part.



**Fig. S1.** EDS1 and EDS2 are EDS profiles of the nanocomposite shown in figure 1(b), in the two areas marked by frames.

## [3]SEM analysis

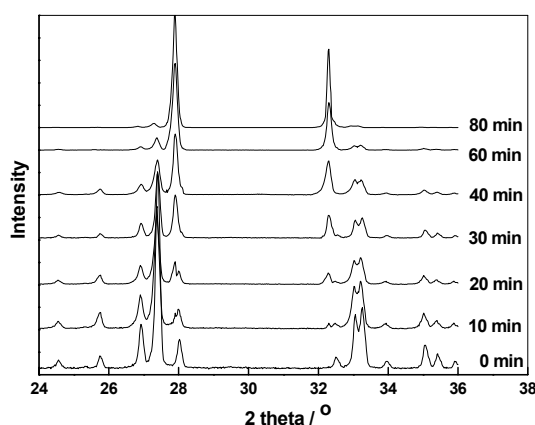
Fig. S2a-c show the SEM images of 3D microjagged  $\text{Bi}_2\text{O}_3$  nanocomposites prepared at 150 °C, 180 °C and 210 °C. It can be observed that only the reaction at 180 °C gave the optimal 3D microjagged  $\text{Bi}_2\text{O}_3$  nanocomposites. The assembly of tooth units showed the disorder and obscure under the preparation condition of 150 °C and 210 °C. This may be attributed that the temperature effect has great influence on the hydrolysis rate of bismuth salt and finally affects the formation of microjagged morphology.



**Fig. S2.** SEM images of 3D microjagged  $\text{Bi}_2\text{O}_3$  nanocomposites prepared at different temperatures. (a) 150 °C, (b) 180 °C and (c) 210 °C

## [4] XRD analysis

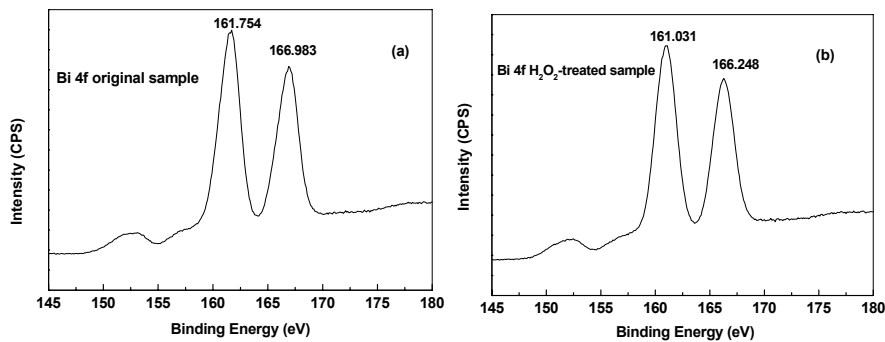
The X-ray diffraction (XRD) profile of the  $\text{H}_2\text{O}_2$ -treated  $\text{Bi}_2\text{O}_3$  shows the presence of a main phase, monoclinic  $\text{Bi}_2\text{O}_3$  ( $\alpha$ - $\text{Bi}_2\text{O}_3$ ), with a minor phase exhibiting two characteristic reflections at  $2\theta = 27.9^\circ$  and  $32.3^\circ$ . The two characteristic reflections can be clearly indexed with the formation of the oxidized  $\text{Bi}_{2-x}\text{O}_3$  species<sup>[1]</sup> on the surface of  $\alpha$ - $\text{Bi}_2\text{O}_3$ . With extending the immersion time, the surface  $\text{Bi}_2\text{O}_3$  phase can be gradually covered by surface  $\text{Bi}_{2-x}\text{O}_3$  phase.



**Fig. S3.** The XRD patterns of the samples treated at different immersion time in  $\text{H}_2\text{O}_2$  solution.

### [5] XPS analysis for the samples

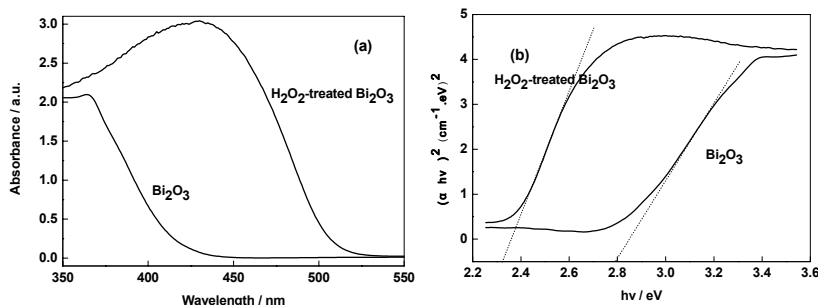
The chemical state transition of surface element was determined by X-ray Photoelectron Spectroscopy (XPS). For bare  $\text{Bi}_2\text{O}_3$ , the peaks located at 161.754 eV and 166.983 eV are assigned to Bi 4f 7/2 and Bi 4f 5/2 region (Fig. S4a). However, it is clear that the corresponding binding energy assigned to Bi 4f 7/2 and Bi 4f 5/2 region shifts to 161.031 eV and 166.428 eV (Fig. S4b) after  $\text{H}_2\text{O}_2$  treatment, suggesting that the surface was highly oxidized and formed  $\text{Bi}_2\text{O}_{4-x}$  species.



**Fig. S4.** The high-resolution XPS spectra of (a) Bi 4f region of pure  $\text{Bi}_2\text{O}_3$  and (b) Bi 4f region of  $\text{H}_2\text{O}_2$ -treated  $\text{Bi}_2\text{O}_3$  samples.

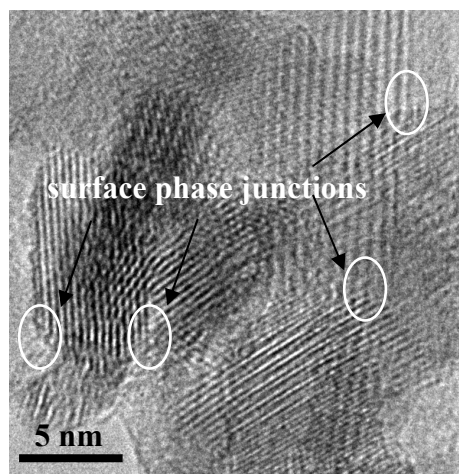
### [6] UV-vis spectra of the samples

Fig. S5 presents the UV/Vis spectra of pure  $\text{Bi}_2\text{O}_3$  and  $\text{H}_2\text{O}_2$ -treated  $\text{Bi}_2\text{O}_3$  samples. The microjagged  $\text{Bi}_2\text{O}_3$  samples are light-yellow in color and the final  $\text{H}_2\text{O}_2$ -treated  $\text{Bi}_2\text{O}_3$  samples appear brown. It is known that the optical absorption coefficient near the band edge follows the equation  $(\alpha h\nu)^2 = A(h\nu - E_g)$  for a direct-bandgap material in which  $\alpha$ ,  $h$ ,  $\nu$ ,  $E_g$ , and  $A$  are the absorption coefficient, Planck constant, light frequency, band gap, and a constant, respectively<sup>[2]</sup>. This relationship gives the band gap ( $E_g$ ) by extrapolating the straight portion of  $(\alpha h\nu)^2$  against  $h\nu$  plot to the point  $\alpha = 0$ , which are about 2.3 eV and 2.8 eV for  $\text{H}_2\text{O}_2$ -treated  $\text{Bi}_2\text{O}_3$  samples and pure  $\text{Bi}_2\text{O}_3$ . The high band gap value of the mixed material can be explained as originating from bulk O(2p)-Bi<sup>3+</sup>(6p<sup>0</sup>) and surface O(2p)-Bi<sup>5+</sup>(6s<sup>0</sup>) transitions made available by  $\text{H}_2\text{O}_2$  treatment.



**Fig. S5.** (a) UV-vis spectrum for the as-prepared  $\text{Bi}_2\text{O}_3$  samples analyzed by the diffuse reflectance method. Adsorption coefficient ( $\alpha$ ) was obtained by the Kubelka-Munk method; (b) the square of adsorption coefficient  $\alpha$  vs. photon energy.

### [7] HRTEM image of the $\text{H}_2\text{O}_2$ -treated $\text{Bi}_2\text{O}_3$ sample



**Fig. S6.** TEM image obtained from a  $\text{H}_2\text{O}_2$ -treated  $\text{Bi}_2\text{O}_3$  sample

#### Reference

- [1] A. Hameed, T. Montini, V. Gombac, P. Fornasiero. *J. Am. Chem. Soc.* **2008**, *130*, 9658–9659.
- [2] M. A. Butler. *J. Appl. Phys.* **1977**, *8*, 1914-1920.